Figure S1

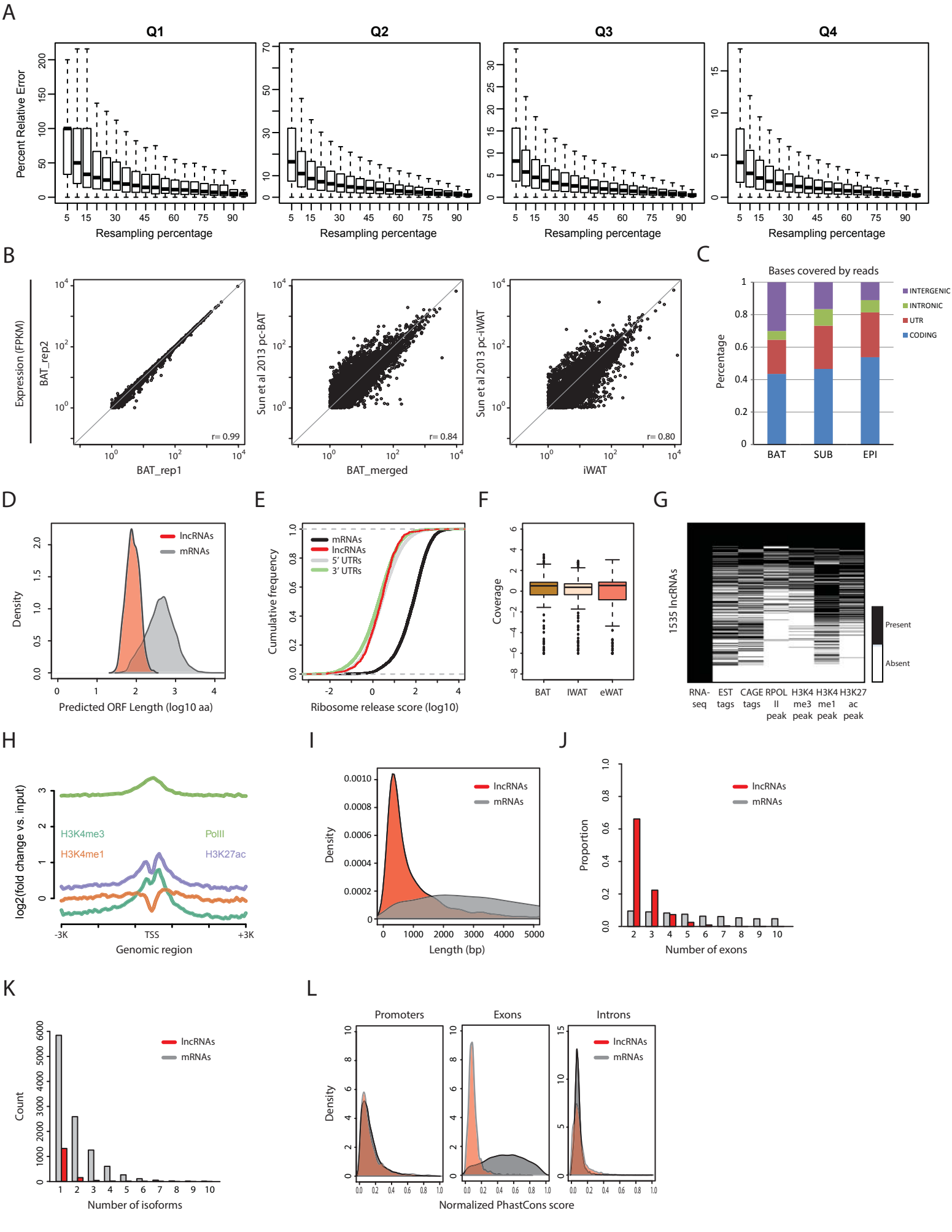
A
Q1
Q2
Q3
Q4
Percent Relative Error
Resampling percentage
B
Expression (FPKM)
BAT_rep2
BAT_rep1
r= 0.99
Sun et al 2013 pc-BAT
BAT_merged
r= 0.84
Sun et al 2013 pc-iWAT
iWAT
r= 0.80
C
Bases covered by reads
Percentage
INTERGENIC
INTRONIC
UTR
CODING
BAT
SUB
EPI
D
lncRNAs
mRNAs
Density
Predicted ORF Length (log10 aa)
E
mRNAs
lncRNAs
5' UTRs
3' UTRs
Cumulative frequency
Ribosome release score (log10)
F
Coverage
BAT
IWAT
eWAT
G
1535 lncRNAs
Present
Absent
RNA-seq
EST tags
CAGE tags
RPOL II peak
H3K4 me3 peak
H3K4 me1 peak
H3K27 ac peak
H
log2(fold change vs. input)
H3K4me3
PolII
H3K4me1
H3K27ac
-3K
TSS
+3K
Genomic region
I
lncRNAs
mRNAs
Density
Length (bp)
J
lncRNAs
mRNAs
Proportion
Number of exons
K
lncRNAs
mRNAs
Count
Number of isoforms
L
Promoters
Exons
Introns
lncRNAs
mRNAs
Density
Normalized PhastCons score

Figure S2

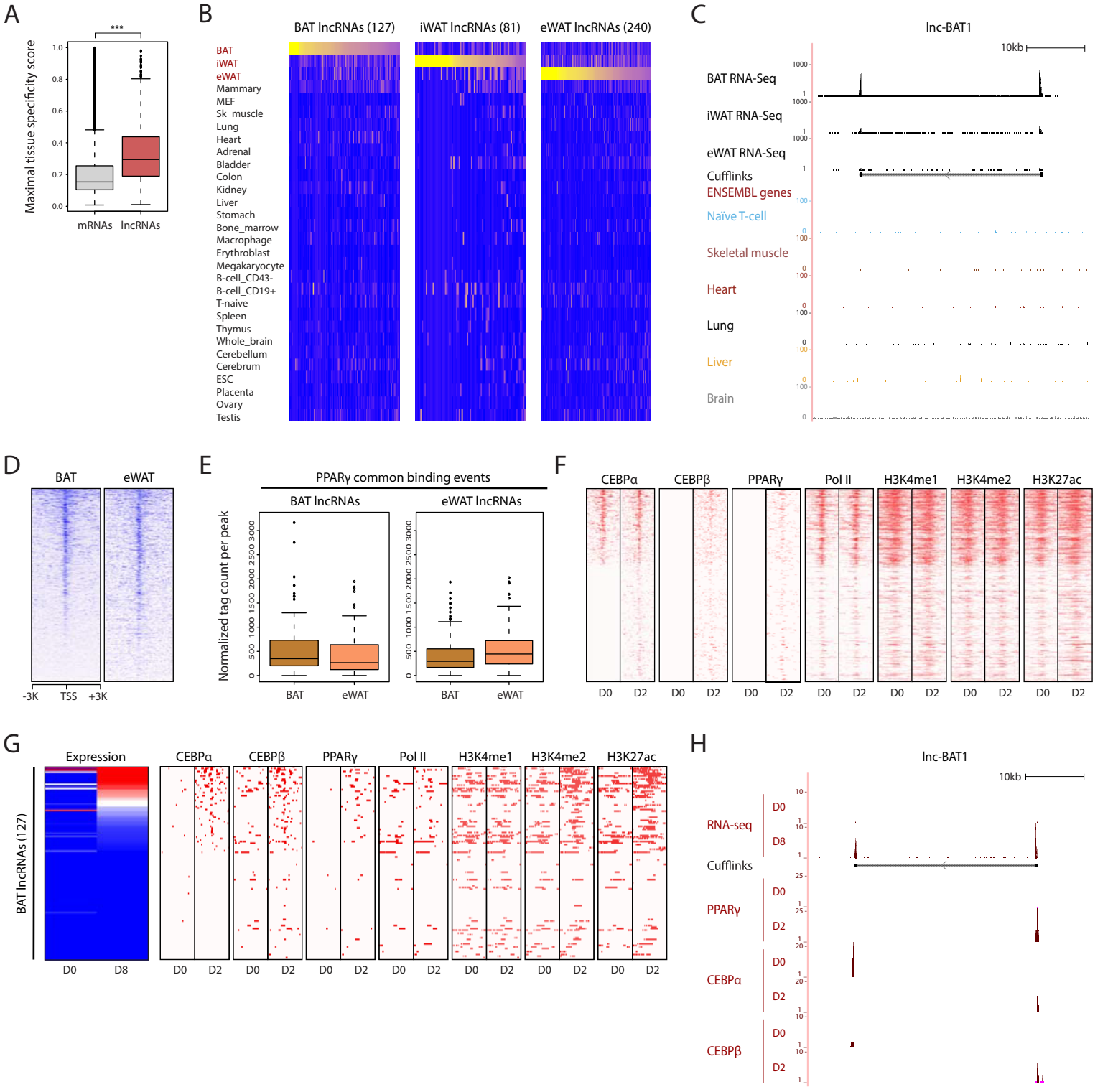
A
***
Maximal tissue specificity score
1.0
0.8
0.6
0.4
0.2
0.0
mRNAs
lncRNAs
B
BAT lncRNAs (127)
iWAT lncRNAs (81)
eWAT lncRNAs (240)
BAT
iWAT
eWAT
Mammary
MEF
Sk_muscle
Lung
Heart
Adrenal
Bladder
Colon
Kidney
Liver
Stomach
Bone_marrow
Macrophage
Erythroblast
Megakaryocyte
B-cell_CD43-
B-cell_CD19+
T-naive
Spleen
Thymus
Whole_brain
Cerebellum
Cerebrum
ESC
Placenta
Ovary
Testis
C
lnc-BAT1
10kb
BAT RNA-Seq
iWAT RNA-Seq
eWAT RNA-Seq
Cufflinks
ENSEMBL genes
Naïve T-cell
Skeletal muscle
Heart
Lung
Liver
Brain
D
BAT
eWAT
-3K
TSS
+3K
E
PPARγ common binding events
BAT lncRNAs
eWAT lncRNAs
Normalized tag count per peak
0
500
1000
1500
2000
2500
3000
BAT
eWAT
F
CEBPα
CEBPβ
PPARγ
Pol II
H3K4me1
H3K4me2
H3K27ac
D0
D2
G
Expression
CEBPα
CEBPβ
PPARγ
Pol II
H3K4me1
H3K4me2
H3K27ac
BAT lncRNAs (127)
D0
D8
D0
D2
H
lnc-BAT1
10kb
RNA-seq
D0
D8
Cufflinks
PPARγ
D0
D2
CEBPα
D0
D2
CEBPβ
D0
D2

Figure S3

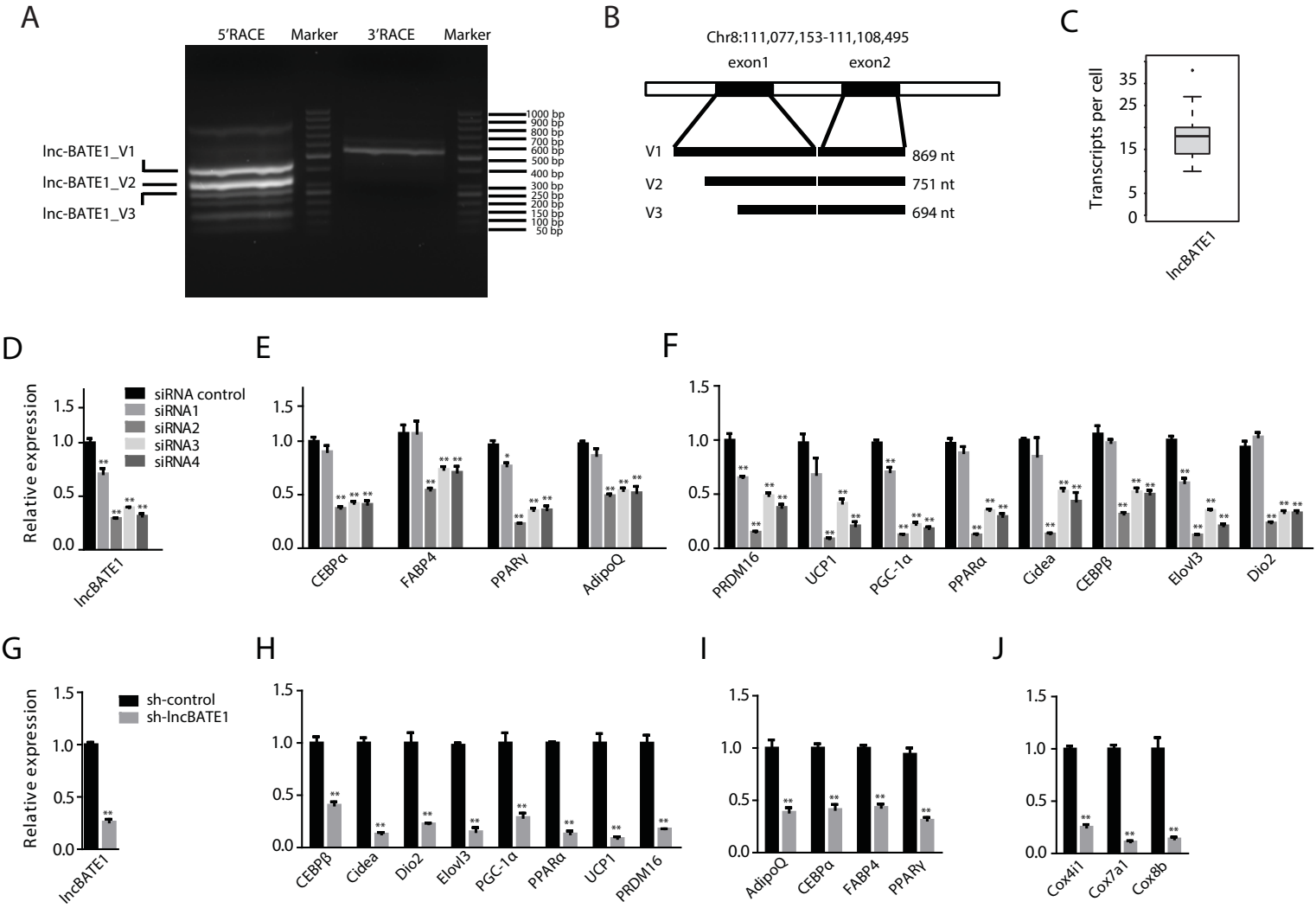
A
5'RACE
Marker
3'RACE
Marker
lnc-BATE1_V1
lnc-BATE1_V2
lnc-BATE1_V3
1000 bp
900 bp
800 bp
700 bp
600 bp
500 bp
400 bp
300 bp
250 bp
200 bp
150 bp
100 bp
50 bp
B
Chr8:111,077,153-111,108,495
exon1
exon2
V1
869 nt
V2
751 nt
V3
694 nt
C
Transcripts per cell
35
25
15
5
0
lncBATE1
D
Relative expression
siRNA control
siRNA1
siRNA2
siRNA3
siRNA4
lncBATE1
E
CEBPα
FABP4
PPARγ
AdipoQ
F
PRDM16
UCP1
PGC-1α
PPARα
Cidea
CEBPβ
Elovl3
Dio2
G
Relative expression
sh-control
sh-lncBATE1
lncBATE1
H
CEBPβ
Cidea
Dio2
Elovl3
PGC-1α
PPARα
UCP1
PRDM16
I
AdipoQ
CEBPα
FABP4
PPARγ
J
Cox4i1
Cox7a1
Cox8b

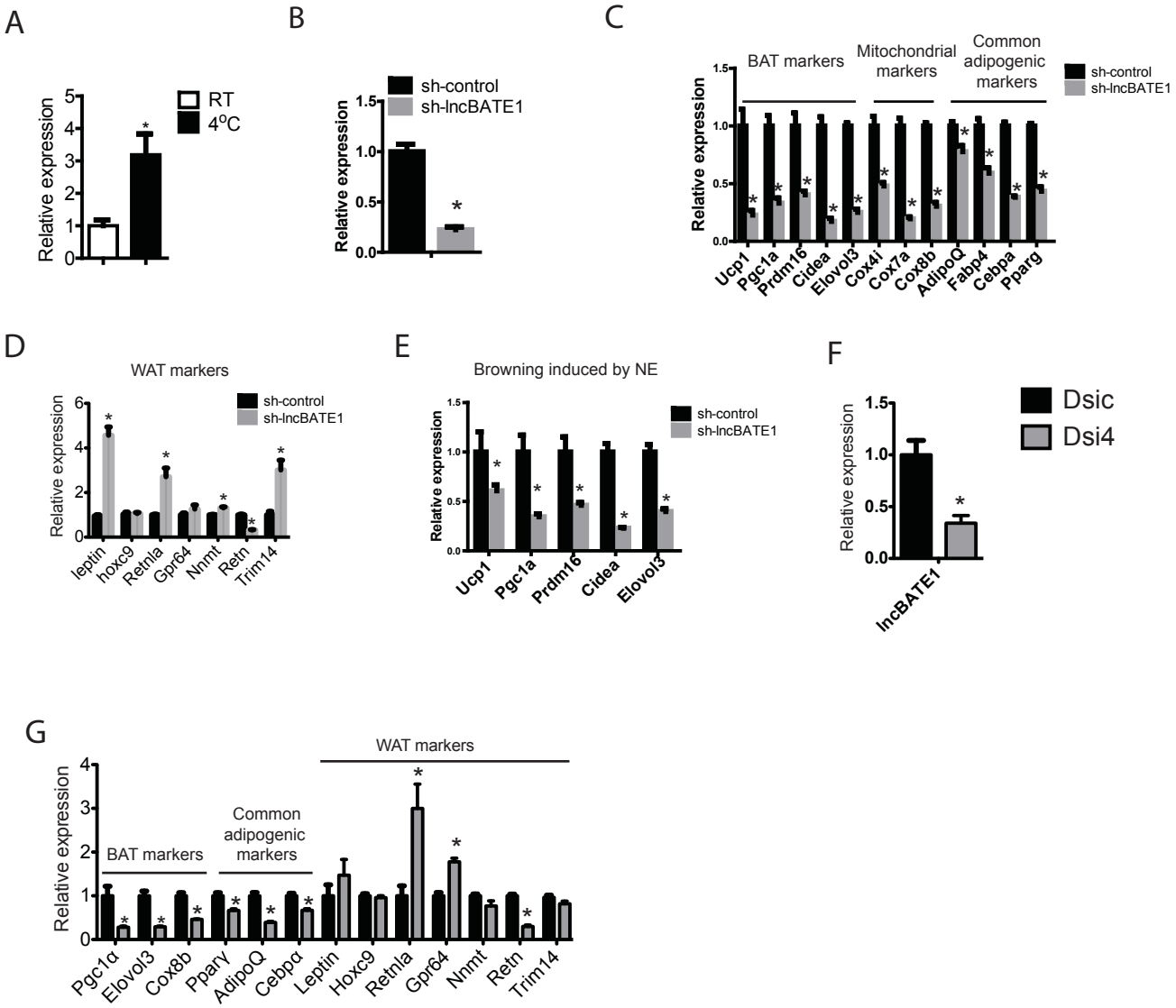
A
Relative expression
RT
4°C
B
sh-control
sh-lncBATE1
Relative expression
C
BAT markers
Mitochondrial markers
Common adipogenic markers
sh-control
sh-lncBATE1
Relative expression
Ucp1
Pgc1a
Prdm16
Cidea
Elovol3
Cox4i
Cox7a
Cox8b
AdipoQ
Fabp4
Cebpa
Pparg
D
WAT markers
sh-control
sh-lncBATE1
Relative expression
leptin
hoxc9
Retnla
Gpr64
Nnmt
Retn
Trim14
E
Browning induced by NE
sh-control
sh-lncBATE1
Relative expression
Ucp1
Pgc1a
Prdm16
Cidea
Elovol3
F
Dsic
Dsi4
Relative expression
lncBATE1
G
WAT markers
BAT markers
Common adipogenic markers
Relative expression
Pgc1α
Elovol3
Cox8b
Pparγ
AdipoQ
Cebpα
Leptin
Hoxc9
Retnla
Gpr64
Nnmt
Retn
Trim14

Figure S5

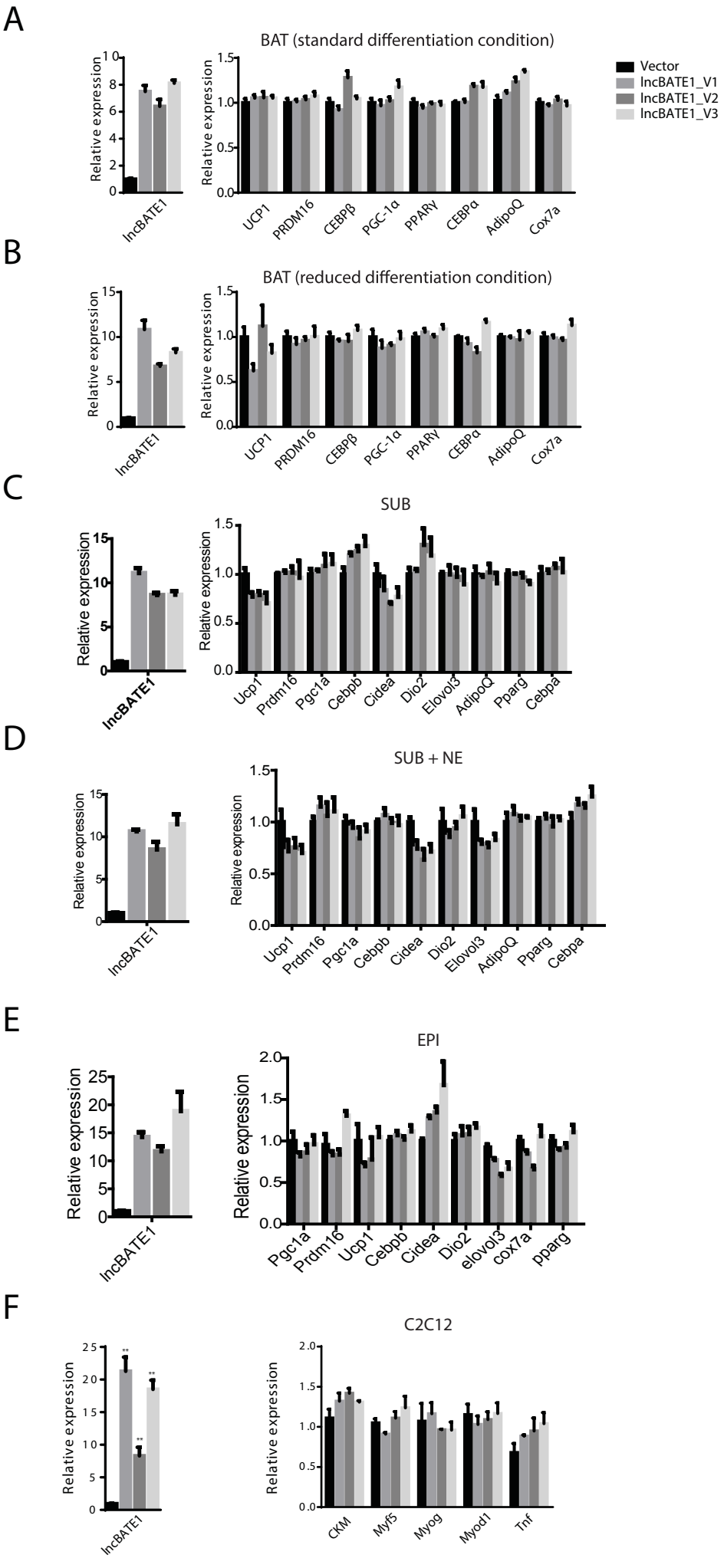
A
BAT (standard differentiation condition)
Relative expression
lncBATE1
UCP1
PRDM16
CEBPβ
PGC-1α
PPARγ
CEBPα
AdipoQ
Cox7a
Vector
lncBATE1_V1
lncBATE1_V2
lncBATE1_V3
B
BAT (reduced differentiation condition)
C
SUB
Ucp1
Prdm16
Pgc1a
Cebpb
Cidea
Dio2
Elovl3
AdipoQ
Pparg
Cebpa
D
SUB + NE
E
EPI
Pgc1a
Prdm16
Ucp1
Cebpb
Cidea
Dio2
elovl3
cox7a
pparg
F
C2C12
CKM
Myf5
Myog
Myod1
Tnf

Figure S6

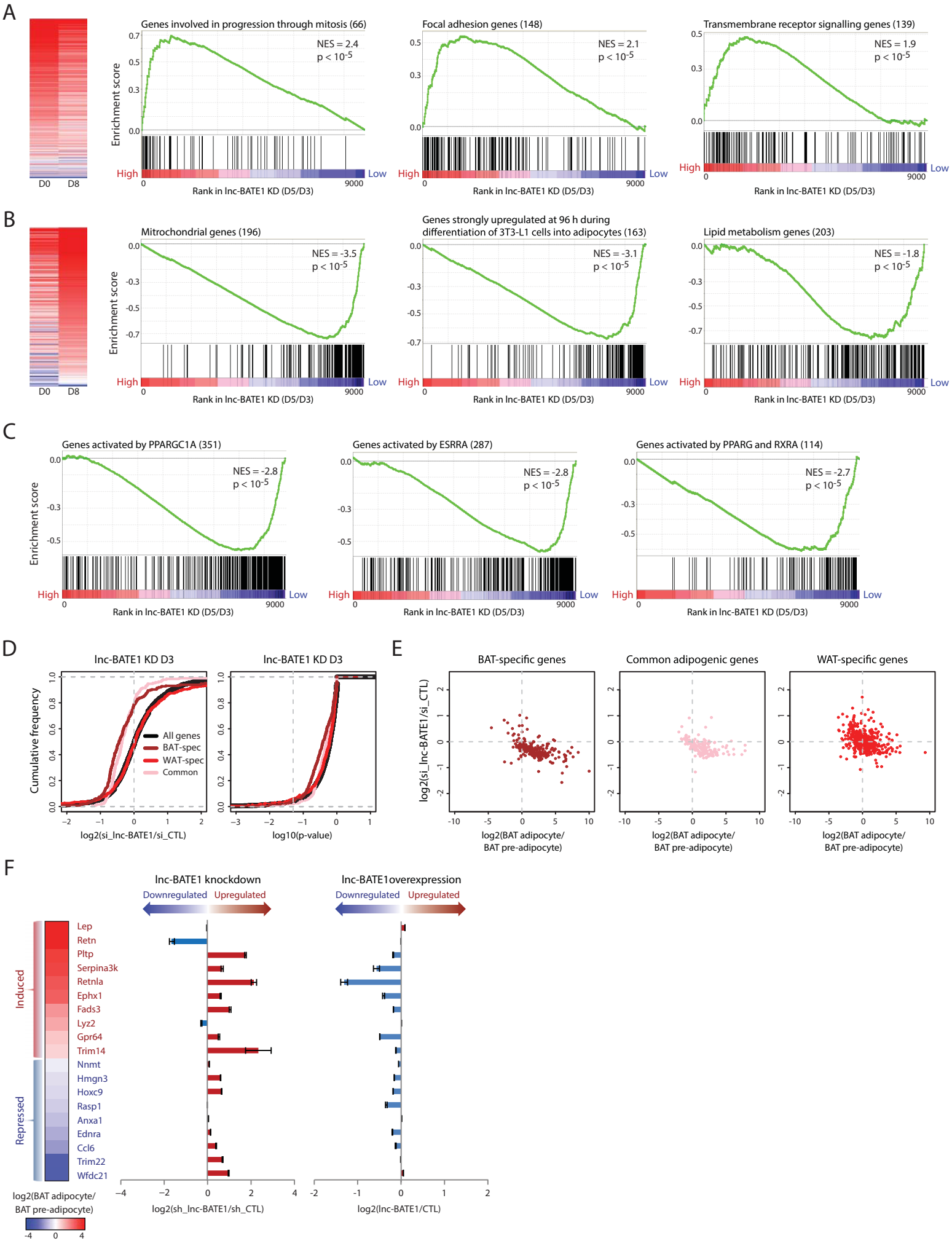
A
Genes involved in progression through mitosis (66)
NES = 2.4
p < 10-5
Focal adhesion genes (148)
NES = 2.1
p < 10-5
Transmembrane receptor signalling genes (139)
NES = 1.9
p < 10-5
Enrichment score
D0 D8
High Low
Rank in lnc-BATE1 KD (D5/D3)
B
Mitrochondrial genes (196)
NES = -3.5
p < 10-5
Genes strongly upregulated at 96 h during differentiation of 3T3-L1 cells into adipocytes (163)
NES = -3.1
p < 10-5
Lipid metabolism genes (203)
NES = -1.8
p < 10-5
C
Genes activated by PPARGC1A (351)
NES = -2.8
p < 10-5
Genes activated by ESRRA (287)
NES = -2.8
p < 10-5
Genes activated by PPARG and RXRA (114)
NES = -2.7
p < 10-5
D
lnc-BATE1 KD D3
Cumulative frequency
All genes
BAT-spec
WAT-spec
Common
log2(si_lnc-BATE1/si_CTL)
log10(p-value)
E
BAT-specific genes
Common adipogenic genes
WAT-specific genes
log2(si_lnc-BATE1/si_CTL)
log2(BAT adipocyte/ BAT pre-adipocyte)
F
lnc-BATE1 knockdown
lnc-BATE1overexpression
Downregulated Upregulated
Induced
Repressed
Lep
Retn
Pltp
Serpina3k
Retnla
Ephx1
Fads3
Lyz2
Gpr64
Trim14
Nnmt
Hmgn3
Hoxc9
Rasp1
Anxa1
Ednra
Ccl6
Trim22
Wfdc21
log2(BAT adipocyte/ BAT pre-adipocyte)
log2(sh_lnc-BATE1/sh_CTL)
log2(lnc-BATE1/CTL)

Figure S7

A

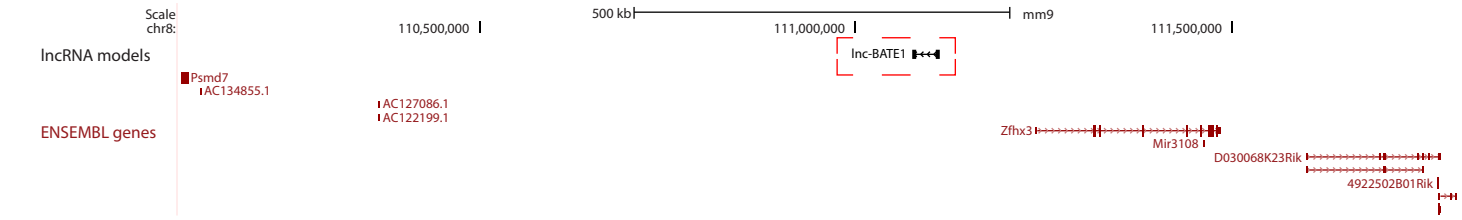

B

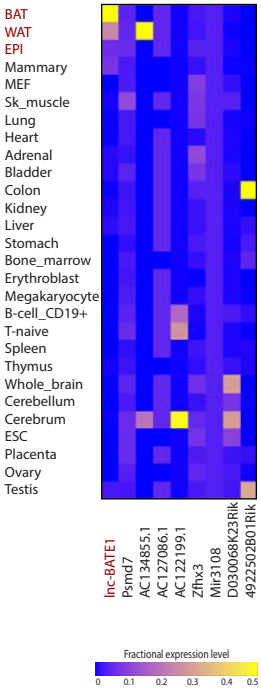

C

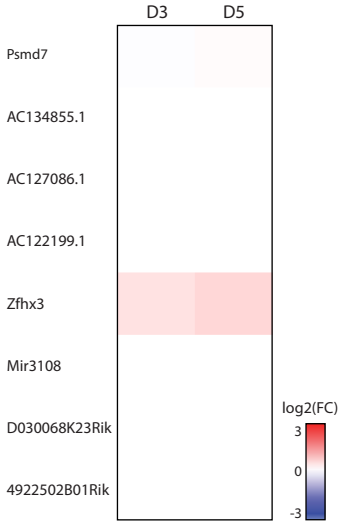

D

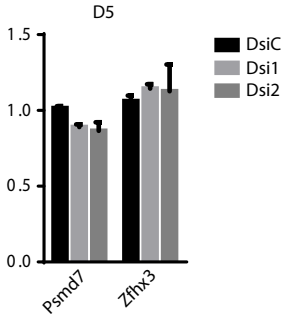

E

putative hnRNP U binding site in lnc-BATE1

UCAGACUUUUUUGUUGCUAUUGAUCUU

Positional weight matrix motif of hnRNPU binding sites

SUPPLEMENTAL FIGURE LEGENDS

Figure S1. Identification and characterization of adipose tissue lncRNAs and their properties, related to Figure 1.

(A) Precision analysis of expression estimates for adipose tissue-expressed genes annotated by Ensembl (43% expressed >1 FPKM in at least one adipose tissue). Box plots depict how the BAT expression level calculated by resampling a series of subsets from the total RNA reads deviates from that estimated using all of the reads, measured as the percent relative error. Transcripts were sorted by their expression value and divided into expression quartiles (Q1-Q4).

(B) Reproducibility analysis of expression estimates for adipose tissue-expressed Ensembl genes as in (A). Correlation of expression levels between BAT replicates from this study (left), between merged BAT replicates from this study and a previously published dataset (Sun et al., 2013) (center), and between iWAT from this study and its previously published counterpart (right).

(C) Distribution of RNA-seq alignment locations relative to RefSeq mRNA annotations.

(D) Maximum predicted ORF length (across all 3 possible reading frames) of adipose-tissue expressed mRNAs and lncRNAs.

(E) Cumulative density distribution of the ribosome release score (Guttman et al., 2013) across adipose tissue-expressed known mRNA ORFs or over any ORF within their 5'UTRs, 3'UTRs, or within lncRNA exons, calculated from RNA-seq and Ribo-seq of mouse 3T3 cells (Shalgi et al., 2013).

(F) Distribution of read coverage values across our adipose tissue samples.

(G) Detection rates for lncRNAs identified in our study. For each lncRNA (rows), detection by the indicated experimental criterion (columns) is indicated in black.

(H) Average profiles of ChIP-seq signal enrichment for histone marks, open chromatin, and RNA Pol II binding within TSS ± 3kb regions of adipose tissue-expressed lncRNAs as in Fig.1F. Color coding for each profile is shown within.

(I) Transcript length distributions for adipose tissue-expressed lncRNAs and mRNAs

(J) Distribution of number of exons per adipose tissue-expressed mRNA or lncRNA transcript

(K) Number of isoforms per adipose-expressed mRNA or lncRNA locus.

(L) Sequence conservation of mRNA or lncRNA promoters (left), exons (center) and introns (right) across 30 vertebrate genomes as measured by Phastcons.

Figure S2. Tissue specificity and regulation of adipose lncRNAs, related to Figure 2.

(A) Distribution of maximal tissue specificity scores for adipose tissue-expressed mRNA or lncRNA genes. ***P <0.001 (Kolmogorov-Smirnov test).

(B) Abundance of BAT-, iWAT- and eWAT-specific lncRNAs across 30 tissues from ENCODE shown as in Fig.2A.

(C) Locus map of lnc-BAT1, a BAT-restricted lncRNA. UCSC genome browser tracks depict poly(A)+ RNA-seq signal (as density of mapped reads in the indicated tissues), *de novo* transcript models by Cufflinks, and Ensembl gene annotations as in Fig.1F.

(D) PPARγ binding in BAT and in eWAT within TSS ± 3kb regions of adipose-expressed lncRNAs. Color intensity represents normalized ChIP-seq signal. Heat maps are sorted in descending order of signal enrichment in the first profile.

(E) Distribution of PPARγ ChIP-seq read counts in BAT or eWAT within peaks of signal enrichment intersecting TSS ± 3kb regions of both BAT- and eWAT-specific lncRNAs. Read counts were quantified by DESeq and common peaks were determined by MACS.

(F) ChIP-seq signal for histone marks, open chromatin and RNA Pol II binding in cultured brown adipocytes within TSS ± 3kb regions of adipose tissue-expressed lncRNAs. Shown are day 0 (D0) and day 2 (D2) time points of brown adipogenesis from immortalized brown pre-adipocytes. Color intensity represents normalized ChIP-seq signal. Heat maps are sorted in descending order of signal enrichment in the first profile.

(G) Heat maps of BAT-specific lncRNA gene-level expression (FPKM) from poly(A)+ RNA-seq of cultured brown adipocytes as in Fig.2D (left) and ChIP-seq signal as in (F) (right).

(H) Locus map of lnc-BAT1 showing activation and TF binding during differentiation. Track 1 depicts poly(A)+ RNA-seq signal as density of mapped reads in cultured brown pre-adipocytes (D0) and cultured brown adipocytes (D8); track 2 depicts *de novo* transcript models by Cufflinks, with right-to-left arrow indicating transcript in the minus strand; tracks 3-5 display PPARγ, CEBPα, CEBPβ ChIP-seq signal as density of processed signal enrichment at days 0 (D0) and 2 (D2) of differentiation from immortalized brown pre-adipocytes in culture.

Figure S3. **lnc-BATE1 inhibition leads to significant down-regulation of key marker genes, related to Figure 4.**

(A) Determination of 5' and 3' ends by RACE reveals 3 variants of lnc-BATE1 in brown adipocytes. Agarose gel image shows 5'RACE and 3'RACE PCR products as indicated.

(B) Gene structure of lnc-BATE1 in mouse genome and its 3 variants.

(C) Quantification of copy number of lnc-BATE1 transcripts per cells based on single molecule FISH data shown in Figure 3D.

(D-F) Expression of lnc-BATE1 (D), common adipogenic markers (E) and brown adipocyte markers (F) in 5-days differentiated brown adipocytes transfected with siRNAs as indicated.

(G-J) Expression of lnc-BATE1 (G), brown adipocyte markers (H), common adipogenic markers (I) and mitochondrial markers (J) in 5-days differentiated brown adipocytes infected with shRNAs as indicated.

Error bars are s.e.m., n =3. *$P \leq 0.05$, **$P \leq 0.01$.

Figure S4. **lnc-BATE1 plays an important role during browning of white adipocytes, related to Figure 4.**

(A) Induction of lnc-BATE1 expression during cold-induced browning of subcutaneous white fat.

(B-D) Inhibition of lnc-BATE1 in inguinal white adipocytes (B) impairs expression of key BAT, mitochondrial, and common adipogenic markers (C) but not WAT markers (D) in the absence of norepinephrine.

(E) Inhibition of lnc-BATE1 in inguinal white adipocytes impairs norepinephrine (NE)-induced thermogenic gene expression.

(F) Inhibition of lnc-BATE1 in epididymal white adipocytes 3 days post-differentiation (F) impairs expression of BAT and common adipogenic but not WAT markers, except for Retn (G). Several BAT markers including Ucp1, Cidea and Prdm16 were not detectable in epididymal adipocyte culture.

Error bars are s.e.m., n =3. *$P \leq 0.05$, **$P \leq 0.01$.

Figure S5. **Ectopic expression of lnc-BATE1 does not stimulate brown adipocyte differentiation or determination, related to Figure 4.**

(A-B) Expression of lnc-BATE1 and BAT marker genes in brown adipocytes differentiated for 5 days under standard conditions (A) or conditions of 10-fold reduced differentiation cocktail (B).

(C-E) Overexpression of lnc-BATE1 is not sufficient to promote browning in cultured inguinal white adipocytes in the absence (C) or presence of norepinephrine (NE) (D) or in cultured epididymal white adipocytes (E).

(F) Expression of lnc-BATE1 and myogenic markers in C2C12 myoblasts differentiated for 6 days.

Error bars are s.e.m., n =3

Figure S6. **Analysis of global gene expression changes upon lnc-BATE1 depletion, related to Figure 5.**

(A) Genes enriched in lnc-BATE1-depleted cells are normally downregulated during brown adipogenesis. Expression estimates (log2 FPKM) in cultured brown adipocytes at differentiation days 0 (D0) and 8 (D8) are shown for genes expressed significantly higher ($P < 0.05$, DESeq) upon lnc-BATE1 inhibition relative to control (left). GSEA identified genes involved in cell cycle progression, cell adhesion, and various signaling processes as significantly enriched within this group (right). Graphical data represent enrichment scores across the genome-wide transcriptional profile (~9000 genes). Genes that are higher-expressed in lnc-BATE1-depeleted cells are presented in red, whereas lower-expressed ones are shown in blue. Number of members in the gene set, normalized enrichment scores and their empirical P values are indicated.

(B) Genes depleted in lnc-BATE1-inhibited cells are normally upregulated during brown adipogenesis. Expression estimates and GSEA analysis as in (A) but for lower-expressed genes.

(C) Genes targeted by PGC1α, ESRRα, and PPARγ are significantly depleted in lnc-BATE1-inhibited cells. GSEA analysis as in (B).

(D) Cumulative density distributions of expression changes (left) and p-values for these changes (right) for all expressed protein-coding genes and for BAT-specific, WAT-specific and common adipogenic genes in siRNA-treated cultured day 3 brown adipocytes. Changes are log2 expression (FPKM) ratios over control siRNA. The 0.05 p-value significance threshold is indicated by a vertical dashed gray line.

(E) Expression changes (log2 FPKM) of BAT-specific, common adipogenic, and WAT-specific protein-coding genes during brown adipogenesis in culture vs. upon lnc-BATE1 knockdown in siRNA-treated cultured day 5 brown adipocytes.

(F) lnc-BATE1 mediates repression of WAT marker genes. Expression change of select WAT markers during brown adipogenesis in culture, shown as the log2 expression ratio between brown adipocytes (Day 6) and pre-adipocytes (Day 0) (left). Expression change in cultured brown adipocytes transfected with shRNA targeting lnc-BATE1 and collected for qPCR at differentiation day 3, relative to control shRNA (middle). Change in expression in cultured day 5

white adipocytes expressing ectopic lnc-BATE1, relative to GFP control (right). Error bars are mean ± SEM., n ≥3.

Figure S7. **Depletion of lncBATE1 does not affect expression of neighboring genes, related to Figure 6.**

(A) Schematic illustration of neighboring genes flanking the lnc-BATE1 locus.

(B) Expression of lnc-BATE1 and neighboring genes across different tissues shown as in Fig.2A.

(C-D) Expression of neighboring genes in 3-days and 5-days differentiated brown adipocytes transfected with DsiRNA2, assessed by RNA-seq (C) and qPCR (D). Error bars are s.e.m., n =3.

(E) Positional weight matrix motif of hnRNP U binding sites identified from previous CLIP-Seq data in human cells (Huelga et al., 2012) is displayed in the top panel. Putative hnRNP U binding site in lncBATE1 is displayed in the bottom panel.

Table S1. List of RNA-seq datasets used in this study, related to Figure 1.

Table S2. List of lncRNA and mRNA groups catalogued in this study, related to Figure 2.

Table S3. Top 5 upstream regulators of genes depleted in lnc-BATE1-inhibited cells, related to Figure 5.

Table S4. Primers, oligos, siRNAs and DsiRNAs used in this study, related to Figure 6.

SUPPLEMENTAL EXPERIMENTAL PROCEDURES

Data sources

The mouse July 2007 (NCBI37/mm9) genome assembly was used throughout the study. Ensembl transcript structures and annotations were obtained from Ensembl version 67 (http://useast.ensembl.org/info/data/ftp/). RefSeq and UCSC transcript structures and annotations were obtained from the UCSC genome browser (March, 2013). We analyzed previously published poly(A)+ RNA-seq reads from primary brown and white adipocytes and from cultured brown adipocytes and pre-adipocytes (Sun et al., 2013), deposited in the Gene Expression Omnibus (GEO; accession number GSE29898). Mouse ENCODE (Stamatoyannopoulos et al., 2012) mapped reads from RNA-seq of poly(A)-selected RNA in 30 primary cells and tissues, from ChIP-seq for histone modifications (H3K4me3, H3K4me1, H3K27ac) in BAT, and from DNase I hypersensitivity in genital fat pad, were downloaded from the mouse ENCODE portal (http://genome.ucsc.edu/ENCODE/downloadsMouse.html). We also analyzed previously published mapped reads from ChIP-seq for histone modifications (H3K4me1, H3K4me2, H3K27ac), transcription factors (CEBPα, CEBPβ, PPARγ) and for serine 5 phosphorylated RNA polymerase II in brown adipocytes derived from immortalized brown pre-adipocytes (Lee et al., 2013), as well as ChIP-seq reads for PPARγ binding in primary BAT and eWAT (Rajakumari et al., 2013). Mapped CAGE tags from the FANTOM3, FANTOM4 and FANTOM5 projects (Carninci et al., 2005; Consortium et al., 2014; Ravasi et al., 2010) were downloaded from the FANTOM website (http://fantom.gsc.riken.jp/4/download/GenomeBrowser/ucsc/mm9/). Mapped poly(A)-seq tags from the Merck Research Laboratories (Derti et al., 2012) were downloaded from the UCSC genome browser (March 2013).

RNA-seq and analysis

Total RNA from primary mouse interscapular brown adipose tissue, epididymal fat pad, and subcutaneous fat pad was isolated using a QIAGEN kit. Sequencing libraries of poly(A)+ RNA from these samples were prepared using the Solexa kit (Illumina) according to the

manufacturer's instructions and sequenced on a Illumina HiSeq2000 sequencer. The resulting 74 bp paired-end reads were quality-checked with FastQC (http://www.bioinformatics.babraham.ac.uk/projects/fastqc/), and low quality reads were removed using the fastq_quality_trimmer ("-t 20 -l 25" parameters) from the FASTX-Toolkit (http://hannonlab.cshl.edu/fastx_toolkit/index.html). Only reads in proper pairs were mapped to mm9 using TopHat v.2.0.4.12 (Trapnell et al., 2009) with default parameters and "--min-anchor 5". The resulting junction files from the BAT, iWAT and eWAT samples were then concatenated and used for another run of TopHat using the --no-novel-juncs parameter. The resulting mapped reads were used to construct *de novo* transcript models using Cufflinks v.2.02 (Trapnell et al., 2010), and the transcript models from each sample were merged using the Cuffmerge utility. We verified that repeating this analysis using only uniquely-mapping reads (86-95% of all reads across our samples) retained 99% of the Cufflinks models identified as lncRNAs by our pipeline, indicating that they do not derive from promiscuous alignment of reads belonging to some other known loci. Transcript- and gene-level expression was quantified by Cufflinks using the Cuffmerge adipose-merged transcriptome, for each fat type and for 30 cell and tissue types from ENCODE. Gene expression in published poly(A)+ RNA-seq data from primary brown and white adipocytes and from cultured brown adipocytes and pre-adipocytes was quantified by Cufflinks using the *de novo* transcript models. Precision of expression estimates was evaluated via resampling using the RPKM_saturation utility from RSeQC (Wang et al., 2012).

lncRNA identification

To retain only reliable transcript models, we considered only multi-exonic transcripts >200bp in length and identified lncRNAs using the following strategy:

1. We implemented a minimal read coverage threshold of >=3 in at least one of the samples. This threshold optimizes the sensitivity and specificity of full length vs. partial length transcript identification based on benchmarking against RefSeq protein-coding or UCSC non-coding gene annotations (Cabili et al., 2011).We verified that coverage value distributions were unbiased across our samples, and obtained similar results using FPKM instead of coverage as a detection threshold.

2. We used BEDTools to intersect *de novo* transcript models with existing transcript models from RefSeq, UCSC and Ensembl, and discarded any transcript overlapping at least 1 bp in the same strand with any annotated mRNA exon, necessary to filter out incompletely assembled mRNAs, unannotated sense-overlapping mRNA isoforms or unannotated 5' or 3' mRNA extensions. We verified our capacity to infer correct strand directionality in our *de novo* transcript models by confirming that 100% of transcripts classified as protein-coding that could be unambiguously assigned to ENSEMBL annotated mRNAs were assigned to the correct strand.
3. For every candidate we retrieved the longest ORF in all three possible frames, using the Sixpack tool from EMBOSS (Rice et al., 2000), and then used HMMER3 (Finn et al., 2011) to query the Pfam A and Pfam B databases (downloaded from ftp://ftp.sanger.ac.uk/pub/databases/Pfam/current_release/ on Nov 2012) with default parameters and discard any transcript with a significant hit (E-value > 0.001). Repeat-masked transcripts were also blasted against the mouse RefSeq protein databases using Blastx (Gish and States, 1993), and transcripts mapping with an E-value <0.0001 were removed.
4. We used PhyloCSF (Lin et al., 2011) to filter out any transcript under evolutionary pressure to preserve synonymous amino acid codons, as judged from its sequence alignment across 29 mammalian genomes. We calculated PhyloCSF scores using "--removeRefGaps --frames=3 --orf=ATGStop" parameters and discarded any transcript with a score >100, corresponding to a 9.3% false negative rate and a 9.7% false positive rate using RefSeq mRNAs and RefSeq lincRNAs as reference.
5. We used the Coding Potential Calculator (Kong et al., 2007) to exclude transcripts with characteristic protein-coding features, independent of their conservation. We calculated CPC scores using default parameters and discarded any transcript with a CPC score >0, corresponding to "coding" or "weakly coding" classifications.
6. We discarded any remaining transcript encoding a peptide (see Mass spectrometry analysis).

Ribosome profiling analysis

We assessed the protein-coding capacity of the lncRNAs in our catalog using the ribosome release criteria (Guttman et al., 2013) based on previously published ribosome profiling data from mouse 3T3 cells (Shalgi et al., 2013). Ribo-seq and RNA-seq reads from untreated 3T3 cells aligned to mm9 were downloaded from GEO (accession number GSE32060).We then used these reads to compute the ribosome release score using the RRS program (http://lncrna.caltech.edu/software/RRS.jar; default parameters and –n "true") for known mRNA ORFs or for all predicted ORFs within our lncRNAs or within mRNA 5' UTRs or 3' UTRs as annotated by Ensembl. Predicted ORFs in all three possible frames were identified using the FindORFs utility (http://lncrna.caltech.edu/software/FindORFs.jar; default parameters and –c "false").

Mass spectrometry analysis

To filter out lncRNAs from our catalog encoding proteins, we searched for peptides predicted from their sequences in a previously published deep mass-spectrometry shotgun coverage of murine brown fat (Huttlin et al., 2010). Mass/charge spectra were analyzed using MaxQuant v.1.4.1.2 (Cox and Mann, 2008). Searches were performed against *in silico* translated peptides from the lncRNA sequences, against the MaxQuant common contaminants database, and against a database comprising all sequences from the mouse Uniprot/Swiss-Prot database. *In silico* translated peptides were retrieved using Sixpack. All searches were run on a Windows server 2008 64bit operating system with 64 CPU blades and 256 GB of RAM using the following general parameters. Parent ion mass tolerance was set to 20ppm, mass tolerance for MS/MS ions was set to 0.02 Da for HCD and to 0.6 Da for CID spectra, minimal peptide length was specified at 6 amino acids, and peptide charge state was limited to +7. Searches had trypsin enzyme specificity, allowing 2 missed cleavages. Asn and Gln deamidation and Met oxidation were included as variable modifications in the search parameters. All peptides were filtered at 1 % FDR. Our search identified 21265 high confidence unique peptides mapping to 3275 mouse Swissprot proteins and 12379 shared peptides mapping to thousands of protein groups. This coverage of the mouse proteome validates both the dataset and the ability of our search to identify peptides present in murine brown fat. We found only 4 peptides whose posterior error probability (PEP) did not exceed 5 %, corresponding to *in silico* translated ORFs from lncRNAs

in our list that were discarded from further consideration. The small number of identified peptides and their relatively large PEP indicate that our strategy for identifying RNA sequences that are not translated has succeeded.

ChIP-seq analysis

Density maps of signal from ChIP-seq for histone modifications, transcription factors, and for serine 5 phosphorylated RNA polymerase II in cultured brown adipocytes and pre-adipocytes (Lee et al., 2013) were retrieved from GEO (accession number GSE50466). We used UCSC utilities and BEDTOOLS to reconstruct mapped reads from these files, and visualized their enrichment at lncRNA promoter-proximal regions (TSS ± 3 kb) using NGSPLOT (Shen et al., 2014). Read counts at these regions were calculated using HTSeq-count (http://www-huber.embl.de/users/anders/HTSeq/doc/index.html) with the "union" mode, and normalized using DESeq (Anders and Huber, 2010). ChIP-seq reads for PPARγ binding in primary BAT and eWAT (Rajakumari et al., 2013) and peak coordinates for BAT- or eWAT-specific binding events were downloaded from GEO (accession number GSE43763), and reads were aligned to mm9 using bowtie2 (Langmead and Salzberg, 2012) with default parameters. We used BEDTOOLS to intersect BAT- and eWAT-specific lncRNA TSS ± 3 kb regions with BAT- and eWAT-specific peaks, defined by Rajakumari et al. by performing peak calling for one depot sample as foreground and the other sample as background. To identify common PPARγ binding peaks, we used mapped reads from BAT or eWAT as input to the peak-calling algorithm MACS (Zhang et al., 2008) using default parameters, the resulting peaks were then pooled and overlapping peaks merged using BEDTOOLS, and any peaks overlapping BAT- and eWAT-specific peaks were discarded. Enrichment of PPARγ at the resulting peaks was quantified by HTSeq-count ("union" mode), and normalized using DESeq.

Global lncRNA validation analysis

To globally validate the lncRNAs identified by our RNA-seq pipeline, we sought independent evidence of expression from the following orthogonal experimental sources:

1. EST and CAGE sequencing tags: we used BEDTools to intersect lncRNA exons with overlapping EST or CAGE tags in the same strand, downloaded from the UCSC database (EST track) or from the FANTOM website (FANTOM4 tag clusters).
2. RNAP II ChIP-seq: we intersected lncRNA TSS ± 3kb regions with binding peaks for RNAP II in day 2 cultured brown adipocytes (Lee et al., 2013), inferred by MACS using default parameters.
3. Histone marks ChIP-seq: we intersected lncRNA TSS ± 3kb regions with enrichment peaks for histone modifications (H3K4me3, H3K4me1, H3K27ac) in BAT, downloaded from ENCODE (Stamatoyannopoulos et al., 2012).

Evolutionary conservation analysis

PhastCons conservation scores based on a 30-way genome alignment seeded with the mouse genome (Blanchette et al., 2004) were downloaded from the UCSC genome browser database for mRNA or lncRNA exons, TSS + 1 kb promoter regions, and introns. The conservation score for the exons, TSS + 1 kb promoter region or introns of a given gene was then obtained by aggregating the PhastCons scores along the region and dividing by the region's total length.

Tissue specificity analysis

Specificity of the expression of a given gene to a given tissue was scored as the fraction of the gene's cumulative expression across tissues represented in that tissue (i.e. its fractional expression level). Tissue specificity scores ranged from 1e-10 to 0.98. We chose an empirical cutoff of 0.15 that optimally distinguishes between known tissue-restricted mRNAs and known uniformly expressed ones and between known BAT-enriched mRNAs and general adipogenic markers, and designated genes scoring above this threshold as tissue-specific. Genes designated as tissue-specific that have BAT, iWAT or eWAT as the tissue with the maximal specificity score were considered BAT-, iWAT- or eWAT-specific, respectively. WAT-specific genes comprised both iWAT- and eWAT-specific genes pooled together. To identify adipose-specific genes common to both BAT and WAT (common adipogenic genes), for each gene we calculated the mean expression value across all non-adipose tissues, and subtracted it from the expression

value in each of BAT, iWAT, and eWAT. We then retained only genes that for each adipose tissue were at least 75 FPKM units above the mean expression value across all non-adipose tissues, an empirical threshold that optimally classified AdipoQ, PPARγ, C/EBPα, FABP4 and Lpl, but not known BAT or WAT markers, as common adipogenic. A small number of genes classified as common adipogenic that were also classified as BAT- or WAT-specific by their tissue specificity scores were kept only in the common adipogenic group. We verified remarkable separation of BAT and WAT tissue specificity score distributions in the BAT- and WAT-specific gene groups, as well as near-identical BAT and WAT distributions in the common adipogenic group.

Single-molecule RNA FISH

Two sets of 34 and 48 DNA 20 nt oligonucleotide probes uniquely mapping along the exons or introns of lnc-BATE1, respectively, were designed using the online designer at http://www.singlemoleculefish.com (version 3.0), with a minimum spacing of 2nt and a target GC content of 45%, applying maximum stringency cutoffs to maximize probe specificity and avoid repetitive and low complexity regions. The probe sequences are available upon request. Probes were synthesized with an amine group at the 3'end (Biosearch Technologies) and coupled to Alexa fluor 594 (Invitrogen) or Cy5.5 (GE Amersham). Fluorophore-coupled probes were ethanol precipitated and purified on an HPLC column. Brown adipocytes cultured in chambered cover glasses (Lab-Tek) were fixed with 1-2 ml of 3.7% (v/v) para-formaldehyde, 1x PBS for 10 minutes at room temperature, and permeabilized by incubating at 4°C in 70% ethanol for at least 16hr. Single-molecule RNA FISH was performed in the chambered cover glasses as described previously (Raj et al., 2008). For hybridization to DNA probes, cells were rehydrated in wash buffer containing 25% (v/v) formamide and 2x SSC for 5min, and then 100µl of hybridization solution, containing labeled DNA probes (2 ng/µl final concentration) in 25% (v/v) formamide, 2x SSC, 1mg/ml BSA, 10mM Vanadyl-ribonucleoside complex, 0.5mg/ml E. coli tRNA and 0.1 g/ml dextran sulfate, were added to the sample and incubated overnight at 37°C. Before imaging, cells were washed twice in 25% (v/v) formamide and 2x SSC for 30min at 37°C, with 5ng/ml DAPI added for the second wash for nuclear counterstaining. For imaging, 200µl of an oxygen-scavenging solution, containing 10mM Tris (pH 7.5), 2x SSC and 0.4% glucose supplemented

with 74µg/ml glucose oxidase, 74µg/ml catalase, and 2mM Trolox, were added to the adherent cells. Images were taken with a Nikon TI-E inverted fluorescence microscope using a 100x oil-immersion objective, custom filters designed to distinguish between different fluorophores, and a Photometrics Pixis 1024 CCD camera (Princeton Instruments) managed by the MetaMorph software (Molecular Devices, Downington, PA). Stacks of images were taken automatically with 0.3µm between z-slices in the Differential Interference Contrast (DIC), DAPI, GFP, AF594 and Cy5 channels. For each biological replicate, at least 10 fields view were imaged. For image processing, the maximum projection of DAPI image z-stacks was merged with the DIC z-slice of maximum contrast and the composite image was used to identify individual cells. AF594 or Cy5 images were compared to GFP control images to detect diffraction-limited spots representing individual RNA transcripts using fixed pixel intensity thresholds. Nuclear vs. cytoplasmic localization was determined manually by visual inspection of merged DAPI and AF594 or Cy5 images. For image presentation, enhanced contrast in the DAPI channel was used to emphasize nuclear counterstaining boundaries.

cDNA synthesis and quantitative real-time PCR

Total RNA from tissue or cell samples was isolated as mentioned above. cDNA was made with random or oligo(dT) primers using M-MLV (Promega). Sybr Green based qPCR was performed in an Applied Biosystems 7900HT Fast Real-time PCR System, using RPL23 as an internal control for normalization.

5’ and 3’ RACE

5’ and 3’ RACE were performed using a FirstChoice RLM-RACE Kit (Life technologies) according to the manufacturer’s instructions. The resulting PCR products were separated on a 1% agarose gel. All visible bands were recovered and cloned into a pGEM-T easy vector. The transcription start and end sites of lncBAT-1 were determined by sequencing >10 colonies with inserts from each band.

Oil-Red-O, Hoechst and Mitotracker Staining

ORO staining was performed as described (Sun et al., 2011). For co-staining of Hoechst and Mitotracker, 5-day differentiated brown adipocytes were stained with 100mM Mitotracker Red FM and 1:5000 dilution of Hoechst at 37°C for 40min. Cell images were captured on an Epson perfection v700 photo scanner for Oil-Red-O staining of whole wells, a Nikon digital sight DS-U3 system for Oil-Red-O cell staining with bright field imaging, and a LECIA DMI3000 B Inverted Microscope for Hoechst and Mitotracker co-staining. For Mitotracker cell fluorescence quantification, the 32-bit full range (0-255) values of images were background-subtracted and analyzed using ImageJ (Schneider et al., 2012). Cells were outlined manually and their area, integrated density and mean gray values measured. Distributions of integrated signal density values were compared using a paired t-test for statistical significance. For image presentation, background-subtracted, 32-bit fluorescence and Hoechst channel images were merged using a linear Look up Table.

Western blot

Cells were collected and lysed in RIPA buffer (50mM Tris-Cl.ph7.4, 1% Triton X-100, 150mM NaCl, 1Mm EDTA, 1mM PMSF, protease inhibitor cocktail). Protein samples were separated on a 4-15% TGX gel (Bio-Rad) and transferred onto a PVDF membrane. The membrane was blocked with 3% BSA in 1XTBST at room temperature for 2h, incubated with a primary antibody overnight at 4°C, and then incubated with a horseradish peroxidase-conjugated secondary antibody for 2h at room temperature. Specific bands were revealed with chemiluminescence substrates and recorded with a ChemDoc MP Image System (Bio-Rad). Primary antibody against Ucp1, hnRNP U, SUZ12, GAPDH were purchased from Abcam. Anti-HuR antibody was purchased from Santa Cruz Biotechnology.

lncRNA Knockdown in mature brown adipocytes

Electroporation of DsiRNA against lnc-BATE1 in mature brown adipocytes was performed in a lonzal 4D-Nucleofactor system using the Amaxa SE cell line 4D-Nucleofactor X Kit with some

program modifications. Briefly, 2X106 differentiated BAT cells were trypsinized, washed with PBS, and re-suspended in electroporation buffer (82ul nucleofactor solution + 18ul supplemental solution). 100 pmol of DsiRNA was added to cells and gently mixed. Cells were transferred to the electroporation cuvette and electroporated using 3T3-L1 (undifferentiated) program with pulse code CA133. After electroporation, cells were incubated at 37 °C for 10 minutes before adding fresh medium and transferring to a culture plate. Growth medium was changed 12 hours after electroporation.

Extracellular Flux Analysis

Primary brown pre-adipocytes were seeded in an X-24 cell culture plate. Cells at 80-90% confluence were then transfected with DsiRNA control or DsiRNA (100uM) targeting lnc-BATE1, grown to full confluence, and induced to differentiate as described (Sun et al., 2013). After 5 days of differentiation, cells were washed with XF-medium in the presence or absence of 2% BSA to block intracellular fatty acid-mediated proton leakage (Li et al., 2014). Oligomycin, Norepinephrine, FCCP and rotene/antimycin were loaded into their respective ports and oxygen consumption rates were measured immediately using the Extracellular Flux Analyzer (Seahorse bioscience) according to the manufacturer's instructions. Oxygen consumption rates were normalized by protein concentration.

Analysis of RNA-seq from lnc-BATE1 knockdown cells

Paired-end 100bp reads from siRNA_lnc-BATE1 or siRNA_Control samples were mapped to mm9 using TopHat v.2.0.4.12 (Trapnell et al., 2009) with default parameters and “--min-anchor 5”. Counts of reads mapping within gene models from Ensembl were obtained using HTSeq-count (http://www-huber.embl.de/users/anders/HTSeq/doc/index.html) with the “union” mode, and normalized using DESeq (Anders and Huber, 2010). Only genes for which a read count could be estimated in each of the samples were considered. Differentially expressed genes ($P < 0.05$ fold-change between lnc-BATE1 and control siRNA, DESeq) in either differentiation stage were used for downstream analysis. Similar downstream analysis results were obtained by using Cuffdiff v2.1.1 instead of DESeq for differential gene expression analysis.

Gene Ontology analysis

Gene lists were analyzed for enrichment of Gene Ontology (GO) terms using DAVID (Huang da et al., 2009a, b). Only Biological Process and Molecular Function terms (GOTERM_BP_FAT and GOTERM_MF_FAT) were considered. To identify the top non-redundant GO terms, we grouped them using the Functional Annotation Clustering tool, and then selected the most significant informative term ($P < 0.05$) within each of the top clusters, ranked by their enrichment score.

Ingenuity Pathway Analysis

Differentially expressed protein-coding genes ($P < 0.05$, DESeq) with lower expression in lnc-BATE1-depleted cells vs. control were analyzed for discovery of regulatory networks using Ingenuity Pathway Analysis (IPA, Ingenuity Systems, Inc., Redwood City, CA). Only experimentally observed direct regulatory relationships were considered for network generation. We used the Upstream Regulator Analysis tool to identify upstream regulators that may be responsible for the gene expression changes in the dataset. This analysis seeks to identify upstream regulators and predict whether they are activated or inhibited given the observed expression changes of their downstream targets, without taking into account expression of the upstream regulators themselves. We focused our analysis on transcription regulators for which an activation state prediction could be generated, and ranked them based on the p-value generated by IPA for their overlap with the expected causal effects on their targets. We then generated a regulatory network based on the known relationships between the top candidate regulators actually present in the dataset and the known target molecules in the dataset used to identify them. The measured expression changes of both regulators and targets in lnc-BATE1-depleted cells vs. control cells were then overlaid on the network. Molecule shapes in the network indicate: ligand-dependent nuclear receptor (rectangle), transcription regulator (ellipse), enzyme (rhombus), transporter (trapezoid), kinase (inverted triangle), and other (circle).

Gene set enrichment analysis

Gene set enrichment analysis (GSEA (Subramanian et al., 2005)) was performed using default parameters and "-metric log2_Ratio_of_Classes", "-permute gene_set", "-nperm 5000". We focused our analysis on curated or pre-ranked gene sets with nominal P <0.05 and empirical FDR <0.25. Enrichment of curated gene sets was analyzed using protein-coding genes differentially expressed (P <0.05, DESeq) in lnc-BATE1-depleted cells vs. control as the expression dataset. The set of genes significantly depleted in lnc-BATE1 KD cells were analyzed for enrichment against the BAT differentiation gene signature previously published (Sun et al., 2013), pre-ranked by the log2 expression change between differentiation days 8 and 0, and against the published gene signature of concurrent genetic deletion of PGC1α and shRNA KD of PGC1β (Uldry et al., 2006), pre-ranked by the log2 expression change between WT and PGC1α KO PGC1β KD. Expression values for the WT and concurrent PGC1α KO PGC1β KD datasets were normalized using GEO2R (http://www.ncbi.nlm.nih.gov/geo/geo2r/).

RNA immunoprecipitation

4-day differentiated primary brown adipocytes grown in 15cm plates were trypsinized, washed, re-suspended in pre-chilled hypotonic buffer, and kept on ice for 15 minutes. Nuclei were released using a glass dounce homogenizer with 10 strokes and pelleted by centrifugation at 2,500g for 15min at 4°C. The supernatant was collected as cytosolic fraction. The pellet was re-suspended in 2ml lysis buffer (25mM hepes, 150mM KCl, 5mM $MgCl_2$, 1mM DTT, protease inhibitor cocktail), and sheared by dounce homogenizer with 50~60 strokes. Nuclear membrane and debris were pelleted and discarded. RNase inhibitor was supplemented in nuclear lysate to a final concentration of 300U/ml before immediate use or storage at -80°C. 30ul Protein A/G beads (SC2003, Santa Cruz) were incubated with 5ug control IgG or indicated antibody in 200ul lysis buffer for 30min at room temperature. Antibody-bound beads were then washed twice in lysis buffer, followed by incubation with 500ul nuclear lysate for 3h at 4°C with continuous rotation. After 4 washes with lysis buffer supplemented with 0.5% NP-40 and 40U/ml RNase inhibitor, 20% of beads were kept for western blot and the rest used for RNA extraction. Bead-

associated RNA was co-precipitated with glycogen and re-suspended in 10ul RNase free H_2O. cDNA synthesis and qPCR were then performed as described above.

RNA pull-down

Biotin-labeled lnc-BATE1 RNA and androgen receptor (AR) 3'UTR RNA were *in vitro* transcribed from PCR fragments harboring a 5' T7 promoter sequence using a MEGAscript kit (Life Technologies) according to the manufacturer's instructions, with a ratio between biotin-CTP and CTP of 1:20. Biotinylated RNAs were further purified with NucAway spin column and re-folded as described previously (Tsai et al., 2010). Magnetic Dynabeads M-280 streptavidin beads (Life Technologies) were pre-treated with 0.1 M NaOH and washed with 0.1M NaCl, and 50ul beads were then incubated with 30pmol biotin-labeled lnc-BATE1 or control RNA in RNA binding buffer (1M NaCl, 5mM Tris) for 30min at R.T. Biotinylated RNA-bound beads were then washed with RNA binding buffer and incubated with brown adipocyte nuclear lysate for 3h at 4°C with continuous rotation. Supernatant and 10% beads were kept for RNA extraction to examine RNA stability during the pull-down assay. Beads were then washed 4 times with wash buffer (25mM hepes, 75mM KCl, 5mM $MgCl_2$, 1mM DTT, protease inhibitor cocktail, 40U/ml RNase inhibitor), and RNA-bound proteins were released by boiling beads in sample buffer for 5 minutes at 95 °C. Protein enrichment was then examined by immunoblotting.

Additional computational methods

Signal density maps were generated using BEDTOOLS (Quinlan and Hall, 2010) and visualized in the UCSC genome browser. Statistical tests and plots were implemented in R (http://www.R-project.org/) with default parameters unless stated otherwise. Expression heatmaps were generated using the heatmap.2 function of the *gplots* R package (http://CRAN.R-project.org/package=gplots).

SUPPLEMENTAL REFERENCES

Anders, S., and Huber, W. (2010). Differential expression analysis for sequence count data. Genome Biol *11*, R106.
Blanchette, M., Kent, W.J., Riemer, C., Elnitski, L., Smit, A.F., Roskin, K.M., Baertsch, R., Rosenbloom, K., Clawson, H., Green, E.D.*, et al.* (2004). Aligning multiple genomic sequences with the threaded blockset aligner. Genome Res *14*, 708-715.
Cabili, M.N., Trapnell, C., Goff, L., Koziol, M., Tazon-Vega, B., Regev, A., and Rinn, J.L. (2011). Integrative annotation of human large intergenic noncoding RNAs reveals global properties and specific subclasses. Genes Dev *25*, 1915-1927.
Carninci, P., Kasukawa, T., Katayama, S., Gough, J., Frith, M.C., Maeda, N., Oyama, R., Ravasi, T., Lenhard, B., Wells, C.*, et al.* (2005). The transcriptional landscape of the mammalian genome. Science *309*, 1559-1563.
Consortium, F., the, R.P., Clst, Forrest, A.R., Kawaji, H., Rehli, M., Baillie, J.K., de Hoon, M.J., Lassmann, T., Itoh, M.*, et al.* (2014). A promoter-level mammalian expression atlas. Nature *507*, 462-470.
Cox, J., and Mann, M. (2008). MaxQuant enables high peptide identification rates, individualized p.p.b.-range mass accuracies and proteome-wide protein quantification. Nat Biotechnol *26*, 1367-1372.
Derti, A., Garrett-Engele, P., Macisaac, K.D., Stevens, R.C., Sriram, S., Chen, R., Rohl, C.A., Johnson, J.M., and Babak, T. (2012). A quantitative atlas of polyadenylation in five mammals. Genome Res *22*, 1173-1183.
Finn, R.D., Clements, J., and Eddy, S.R. (2011). HMMER web server: interactive sequence similarity searching. Nucleic Acids Res *39*, W29-37.
Gish, W., and States, D.J. (1993). Identification of protein coding regions by database similarity search. Nat Genet *3*, 266-272.
Guttman, M., Russell, P., Ingolia, N.T., Weissman, J.S., and Lander, E.S. (2013). Ribosome Profiling Provides Evidence that Large Noncoding RNAs Do Not Encode Proteins. Cell *154*, 240-251.
Huang da, W., Sherman, B.T., and Lempicki, R.A. (2009a). Bioinformatics enrichment tools: paths toward the comprehensive functional analysis of large gene lists. Nucleic Acids Res *37*, 1-13.
Huang da, W., Sherman, B.T., and Lempicki, R.A. (2009b). Systematic and integrative analysis of large gene lists using DAVID bioinformatics resources. Nat Protoc *4*, 44-57.
Huttlin, E.L., Jedrychowski, M.P., Elias, J.E., Goswami, T., Rad, R., Beausoleil, S.A., Villen, J., Haas, W., Sowa, M.E., and Gygi, S.P. (2010). A tissue-specific atlas of mouse protein phosphorylation and expression. Cell *143*, 1174-1189.
Kong, L., Zhang, Y., Ye, Z.Q., Liu, X.Q., Zhao, S.Q., Wei, L., and Gao, G. (2007). CPC: assess the protein-coding potential of transcripts using sequence features and support vector machine. Nucleic Acids Res *35*, W345-349.
Langmead, B., and Salzberg, S.L. (2012). Fast gapped-read alignment with Bowtie 2. Nat Methods *9*, 357-359.
Lee, J.E., Wang, C., Xu, S., Cho, Y.W., Wang, L., Feng, X., Baldridge, A., Sartorelli, V., Zhuang, L., Peng, W.*, et al.* (2013). H3K4 mono- and di-methyltransferase MLL4 is required for enhancer activation during cell differentiation. Elife *2*, e01503.
Li, Y., Fromme, T., Schweizer, S., Schottl, T., and Klingenspor, M. (2014). Taking control over intracellular fatty acid levels is essential for the analysis of thermogenic function in cultured primary brown and brite/beige adipocytes. EMBO Rep *15*, 1069-1076.
Lin, M.F., Jungreis, I., and Kellis, M. (2011). PhyloCSF: a comparative genomics method to distinguish protein coding and non-coding regions. Bioinformatics *27*, i275-282.
Quinlan, A.R., and Hall, I.M. (2010). BEDTools: a flexible suite of utilities for comparing genomic features. Bioinformatics *26*, 841-842.
Raj, A., van den Bogaard, P., Rifkin, S.A., van Oudenaarden, A., and Tyagi, S. (2008). Imaging individual mRNA molecules using multiple singly labeled probes. Nat Methods *5*, 877-879.

Rajakumari, S., Wu, J., Ishibashi, J., Lim, H.W., Giang, A.H., Won, K.J., Reed, R.R., and Seale, P. (2013). EBF2 determines and maintains brown adipocyte identity. Cell Metab *17*, 562-574.
Ravasi, T., Suzuki, H., Cannistraci, C.V., Katayama, S., Bajic, V.B., Tan, K., Akalin, A., Schmeier, S., Kanamori-Katayama, M., Bertin, N.*, et al.* (2010). An atlas of combinatorial transcriptional regulation in mouse and man. Cell *140*, 744-752.
Rice, P., Longden, I., and Bleasby, A. (2000). EMBOSS: the European Molecular Biology Open Software Suite. Trends Genet *16*, 276-277.
Schneider, C.A., Rasband, W.S., and Eliceiri, K.W. (2012). NIH Image to ImageJ: 25 years of image analysis. Nat Methods *9*, 671-675.
Shalgi, R., Hurt, J.A., Krykbaeva, I., Taipale, M., Lindquist, S., and Burge, C.B. (2013). Widespread regulation of translation by elongation pausing in heat shock. Molecular cell *49*, 439-452.
Shen, L., Shao, N., Liu, X., and Nestler, E. (2014). ngs.plot: Quick mining and visualization of next-generation sequencing data by integrating genomic databases. BMC Genomics *15*, 284.
Stamatoyannopoulos, J.A., Snyder, M., Hardison, R., Ren, B., Gingeras, T., Gilbert, D.M., Groudine, M., Bender, M., Kaul, R., Canfield, T.*, et al.* (2012). An encyclopedia of mouse DNA elements (Mouse ENCODE). Genome Biology *13*.
Subramanian, A., Tamayo, P., Mootha, V.K., Mukherjee, S., Ebert, B.L., Gillette, M.A., Paulovich, A., Pomeroy, S.L., Golub, T.R., Lander, E.S.*, et al.* (2005). Gene set enrichment analysis: a knowledge-based approach for interpreting genome-wide expression profiles. Proc Natl Acad Sci U S A *102*, 15545-15550.
Sun, L., Goff, L.A., Trapnell, C., Alexander, R., Lo, K.A., Hacisuleyman, E., Sauvageau, M., Tazon-Vega, B., Kelley, D.R., Hendrickson, D.G.*, et al.* (2013). Long noncoding RNAs regulate adipogenesis. Proc Natl Acad Sci U S A *110*, 3387-3392.
Sun, L., Xie, H., Mori, M.A., Alexander, R., Yuan, B., Hattangadi, S.M., Liu, Q., Kahn, C.R., and Lodish, H.F. (2011). Mir193b-365 is essential for brown fat differentiation. Nat Cell Biol *13*, 958-965.
Trapnell, C., Pachter, L., and Salzberg, S.L. (2009). TopHat: discovering splice junctions with RNA-Seq. Bioinformatics *25*, 1105-1111.
Trapnell, C., Williams, B.A., Pertea, G., Mortazavi, A., Kwan, G., van Baren, M.J., Salzberg, S.L., Wold, B.J., and Pachter, L. (2010). Transcript assembly and quantification by RNA-Seq reveals unannotated transcripts and isoform switching during cell differentiation. Nat Biotechnol *28*, 511-515.
Tsai, M.C., Manor, O., Wan, Y., Mosammaparast, N., Wang, J.K., Lan, F., Shi, Y., Segal, E., and Chang, H.Y. (2010). Long noncoding RNA as modular scaffold of histone modification complexes. Science *329*, 689-693.
Uldry, M., Yang, W., St-Pierre, J., Lin, J., Seale, P., and Spiegelman, B.M. (2006). Complementary action of the PGC-1 coactivators in mitochondrial biogenesis and brown fat differentiation. Cell Metab *3*, 333-341.
Wang, L., Wang, S., and Li, W. (2012). RSeQC: quality control of RNA-seq experiments. Bioinformatics *28*, 2184-2185.
Zhang, Y., Liu, T., Meyer, C.A., Eeckhoute, J., Johnson, D.S., Bernstein, B.E., Nusbaum, C., Myers, R.M., Brown, M., Li, W.*, et al.* (2008). Model-based analysis of ChIP-Seq (MACS). Genome Biol *9*, R137.